CHALMERS
UNIVERSITY OF TECHNOLOGY

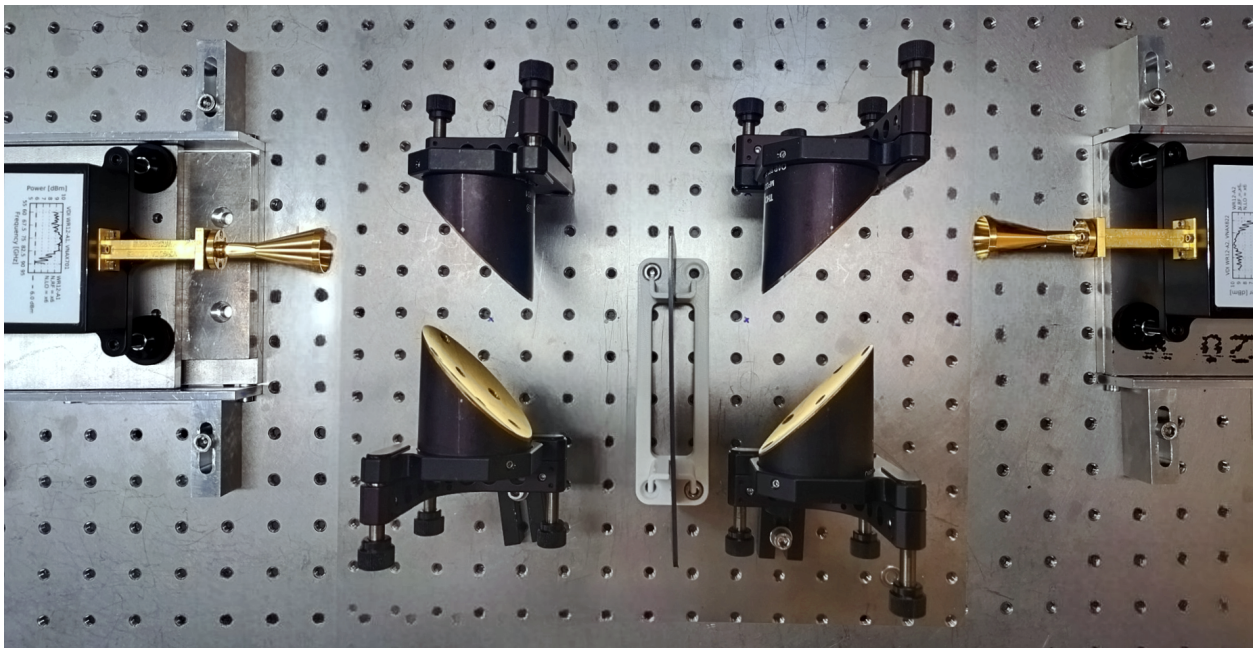

Characterisation of Recycled Plastics for Automotive Radar Applications at 77 GHz

Master of Science thesis in the Master's programme of Communication Engineering

MOHAMED AZAD AMEERUDEEN

MOHAMMAD NOURJOO

DEPARTMENT OF ELECTRICAL ENGINEERING

CHALMERS UNIVERSITY OF TECHNOLOGY
Gothenburg, Sweden 2024
www.chalmers.se

Master's thesis 2024

Characterisation of Recycled Plastics for Automotive Radar Applications at 77 GHz

MOHAMED AZAD AMEERUDEEN

MOHAMMAD NOURJOO

CHALMERS
UNIVERSITY OF TECHNOLOGY

Department of Electrical Engineering
Chalmers University of Technology
Gothenburg, Sweden 2024

Characterisation of Recycled Plastics for Automotive Radar Applications at 77 GHz
Master's thesis in the Master's programme of Communication Engineering
MOHAMED AZAD AMEERUDEEN
MOHAMMAD NOURJOO

Examiner : Prof. Dr. Jan Stake, Head of Division,
Terahertz and Millimetre Wave Laboratory,
Department of Microtechnology and Nanoscience,
Chalmers University of Technology, Gothenburg, Sweden

Supervisor : Dr. Stella Bevilacqua, Radar Group,
Engr. Sara Tell, Radar Group,
Dr. Iman Vakili, Radar Group,
Volvo Cars, Gothenburg, Sweden

Master's Thesis 2024
Department of Electrical Engineering
Chalmers University of Technology
SE-412 96 Gothenburg
Telephone +46 31 772 1000

Cover: Photo of quasi-optical measurement setup consisting of frequency extenders and parabolic mirrors.

Typeset in LaTeX \tagtemp\ Printed by Chalmers Reproservice
Gothenburg, Sweden 2024

Characterisation of Recycled Plastics for Automotive Radar Applications at 77 GHz

MOHAMED AZAD AMEERUDEEN
MOHAMMAD NOURJOO
Department of Electrical Engineering
Chalmers University of Technology

Abstract

This work investigates the potential of various recycled plastic materials for use in bumper areas which are in closer proximity to automotive radar systems operating at 77 GHz. The study focuses on both experimental and analytical calculation approaches to assess the electromagnetic properties of these materials, specifically focusing on their complex permittivity and loss tangent characteristics at 77 GHz. For this purpose, a quasi-optical measurement setup which utilises metallic reflective mirrors to narrow and collimate the beam of waves produced by WR12 frequency extenders in the 65-90 GHz range is used. The S-parameters measured by the Vector Network Analyzer (VNA) of the samples are utilised to calculate the complex refractive index. This procedure allows for the determination of the permittivity and loss tangent for each specific sample material. To ensure the robustness of the calculation method, the known permittivity and loss tangent values at 77 GHz from a reference non-recycled material provided by the supplier are utilised to calculate theoretical S-parameters, which are then employed in the same method to re-evaluate the permittivity and loss tangent. This process enables a direct comparison with the initial VNA-derived results. This round-trip verification process confirms the reliability of the calculation method used in the analysis. From the analysis of all test materials, a particular recycled plastic material is chosen, suggesting its potential suitability for use in automotive bumper production. Overall, this research o□ers significant insights into the development of radar-compatible recycled plastics for bumper design and manufacturing.

Keywords: Automotive radar, recycled plastics, metallic reflective mirrors, S-parameters, Quasi-optical technique, refractive index, permittivity and loss tangent.

Acknowledgements

We would like to express our heartfelt gratitude to our Manager, Lucia Dascola, for entrusting us with this opportunity, as well as the invaluable support provided by our Supervisors, Dr. Stella Bevilacqua, Engr. Sara Tell and Dr. Iman Vakili at Volvo Cars. We are deeply thankful for the guidance of our Examiner, Professor Dr. Jan Stake, whose expertise and mentorship have been invaluable throughout our entire thesis. We extend our special appreciation to Dr. Anis Moradikouchi and Divya Jayasankar, Researchers from the Department of Microtechnology and Nanoscience at Chalmers University of Technology, for their uttermost assistance and guidance.

We are very fortunate to have worked along with the Radar Group at Volvo Cars throughout our entire thesis. Their constant support and appreciation, deeply helped us to be more proficient and diligent in our work. We also want to thank our friends in 6th floor of MC2 for all the help and fun time we had. Last but not least, we are extremely delighted to convey our heartfelt thanks to our family and friends for their unquenchable love and support.

MOHAMED AZAD AMEERUDEEN
MOHAMMAD NOURJOO
8th January 2024

List of acronyms

Below is the list of acronyms that have been used throughout this thesis listed in alphabetical order:

ABS	Acrolynitrile Butadiene Styrene
ADAS	Advanced Driver Assistance Systems
AEB	Automatic Emergency Braking
ATC	Air Tra□c Control
HDPE	High-density polyethylene
LDPE	Low-density polyethylene
MUT	Material Under Test
PA	Polyamides
PC	Polycarbonate
PE	Polyethylene
PET	Polyethylene Terephthalate
PMMA	Polymethyl Methacrylate
POM	Polyoxy
PP	Polypropylene
PPS	Polyphenylene sulfide
PS	Polystyrene
PU	Polyurethane
PVC	Polyvinyl Chloride
RADAR	Radio Detection and Ranging
SNR	Signal to Noise ratio
SOLT	Short, Open, Load, Thru
TEM	Transverse Electromagnetic
VNA	Vector Network Analyzer

Nomenclature

Below is the nomenclature of indices, sets, parameters, and variables that have been used throughout this thesis.

Indices

j	Imaginary unit, $\sqrt{-1}$

Parameters

ε	Permittivity
ε_r	Relative permittivity
ε_0	Permittivity of free space
ε	Real part of permittivity
ε	Imaginary part of permittivity
Z_0	Impedance of free-space
μ_0	Permeability of free space
μ_r	Relative permeability
c	Speed of light

Variables

ω	Angular frequency
$\tilde{n}$	Refractive index
n	Real part of refractive index
κ	Imaginary part of refractive index
k_0	Free-space wave number
f	Frequency

Z	Impedance of media
$\tan\delta$	Loss tangent
ϕ	Phase of transmission
z_R	Rayleigh range
Γ	Reflection coe□cient
d	Thickness of MUT
τ	Time delay
T	Transmission coe□cient
λ	Wavelength

Contents

List of figures

List of tables

1

Introduction

Modern-day automobiles have become more advanced in every phase of technology than the automobiles that were in use over the past two decades. They are constantly upgraded both in design and underlying technology to support multiple new features including full autonomous functionality. To support these new features, modifications are made in both hardware and software phases to provide comfort for the passengers by providing minimal control over the vehicle and avoiding possible accidents or injuries due to human error. This functionality is widely termed Advanced Driver Assistance Systems (ADAS) in the automobile industry.

1.1 Automotive radars

Radar, which stands for Radio Detection and Ranging [1], was initially developed for military purposes and later adapted for civilian applications, including Air traffic control (ATC), weather monitoring, remote sensing, and later on automotive usage. Automotive radars play a pivotal role in detecting and tracking objects at various speeds and distances, ranging from a few meters to several hundred meters. Their high sensitivity enables accurate detection of even small objects.

Precise angular measurements are essential, as they determine an object's location and movement relative to the vehicle. With range resolution and accuracy being inversely proportional to the sweep bandwidth. When compared to 24 GHz radar, a 77 GHz radar sensor may reach x4 greater performance in terms of accuracy and range resolution because a maximum of 1 GHz bandwidth is being used. The radar continuously monitor the surrounding environment, providing invaluable data for ADAS and autonomous driving systems.

With the advent of ADAS, Radar became an integral part of complex safety systems. They are now utilised in functions like Automatic Emergency Braking (AEB), blind-spot detection, lane-change assist, and rear cross-traffic alert. These functions utilise radar to sense and analyse the environment, providing drivers with enhanced situational awareness and assisting in avoiding potential accidents. Automotive radar, cameras, and lidar are used in combination to create a comprehensive perception system in automotive applications, with radar proving particularly useful in low-light conditions where cameras may struggle, providing viable solutions for maintaining perception and safety in such environments.

1.2 Recycled plastics

Governments and regulatory bodies around the world have imposed stricter environmental regulations, including mandates to reduce waste and promote recycling. These regulations have compelled automobile manufacturers to explore more sustainable materials like recycled plastics for interior components and body panels, as well as other innovative solutions such as bio-based composites, lightweight alloys, and advanced coatings that not only meet performance and safety standards but also reduce the environmental impact of vehicle production and operation. Recycled plastics are often more affordable than virgin plastics, enabling manufacturers to reduce production costs and enhance their profitability. The automotive industry demands high-performance materials that can withstand rigorous conditions such as strength, durability, heat resistance, and impact resistance, to be suitable for automotive applications which requires the availability of a consistent supply of high-quality recycled plastics. An efficient collection, sorting, and recycling infrastructure must be established to ensure a steady stream of recycled plastic materials for automobile manufacturers.

As far as the introduction of recycled plastics into the automotive industry, 7 types of recycled plastics were identified and classified for their composition and percentage of recyclability. They are Polyethylene Terephthalate (PET), High-density polyethylene (HDPE), Polypropylene (PP), Low-density polyethylene (LDPE), Polyvinyl Chloride (PVC), Polystyrene (PS), and Others (materials that can't be recycled through common recycling bins). The end use can differ depending on the type of recyclable plastic [2]. Moreover, 39 types of basic polymers and plastics are employed in the manufacturing of an automobile. The most commonly used ones out of a total of 74% of plastics are PP about 35% (in bumpers, cable insulation carpet fibres, etc.), Polyurethane (PU) about 19% (eg., foam seating, insulation panels, suspension bushings, cushions, electrical compounds, etc.), Polyamides (PA) about 11% (eg., battery casings, brake hoses, oil sumps, etc.,) and PVC about 9% (eg., instrument panels, electrical cables, pipes, doors, etc.). Other engineering plastics, such as Acrylonitrile Butadiene Styrene (ABS), PS, Polyethylene (PE), Polyoxymethylene (POM), Polycarbonate (PC), Polymethyl Methacrylate (PMMA), etc., are used as a combination for other vehicle parts [3]. Most of the materials that are analyzed in this thesis are of made of PP, PC or Polyphenylene sulfide (PPS).

1.3 Purpose of research

Recycled plastics exhibit unique material properties due to variations in composition and manufacturing processes. These discrepancies can significantly affect radar and other sensors, leading to issues like unwanted signal propagation, signal attenuation, phase shifts, missed detections, and false alarms. The motivation behind this research is the increasing necessity to understand how radar systems function when placed behind bumpers made of recycled materials. Given the limited data on the characteristics of recycled plastic materials and their impact on radar performance, there is an urgent need for detailed research in this area. This involves a thorough material characterisation of recycled plastics, comparing their properties to conven-

tional plastics by analysing aspects such as permittivity, loss tangent, conductivity etc, It's also vital to understand how these properties are a□ected under varying conditions, like temperature and humidity. Practical radar system tests are equally important to pinpoint real-world performance challenges and devise appropriate solutions. Therefore, understanding and addressing the challenges posed by recycled plastics in this domain is of higher importance.

1.4 Scope

In this thesis, the dielectric properties of the recycled plastics are measured using a quasi-optical setup which includes metallic reflective mirrors to collimate the beam to a narrow focus, thereby ensuring accurate and consistent readings. From the S-parameters obtained through the Vector Network Analyzer (VNA), the refractive index is calculated which in turn gives the permittivity and loss tangent of all the test materials in the E-band (65-90 GHz). Reference material with known permittivity and loss tangent is used to verify the robustness of the calculation method used in this thesis. Also, the dielectric properties of all the test materials are calculated through an analytical method which helps to pinpoint and rectify any potential configuration anomalies in the setup, thereby ensuring that the permittivity extraction software functions with the utmost precision and accuracy in determining the complex permittivity of the test material.

2

Theory

2.1 Dielectric Characterisation

In the realm of material science and electromagnetic theory, refractive index (n), complex permittivity (ε) and loss tangent ($\tan\delta$) are the fundamental parameters that depict how a material behaves in an electromagnetic field.

2.1.1 Refractive index

The refractive index (n) of a medium describes how much the speed of light (or electromagnetic waves) is reduced inside the medium compared to the speed of light in a vacuum. The refractive index is defined as:

$$n = \frac{c}{v} \tag{2.1}$$

where,

c is the speed of light in a vacuum (approximately 3×10^8 m/s) and

v is the speed of light in the medium.

For materials that have both electric and magnetic responses to an electromagnetic field, the refractive index can be related to the relative permittivity (ε_r) and relative permeability (μ_r) of the medium by:

$$n = \sqrt{\varepsilon_r \mu_r} \tag{2.2}$$

However, in many practical cases (especially at optical frequencies), the magnetic response (μ_r) for a non-magnetic sample material is approximately equal to 1, and hence the relation becomes:

$$n \approx \sqrt{\varepsilon_r} \tag{2.3}$$

When a Material Under Test (MUT) is exposed to an electromagnetic field, the analysis of the wave propagation behaviour, characterised by parameters such as wavelength, frequency, and amplitude, within the material becomes essential for accurately determining the MUT's dielectric properties. One e□ective method, according to principles of photonics and guided by established research [4] [5], is by precisely measuring the complex refractive index ($\tilde{n}$) of the MUT.

$$\tilde{n} = n - j\kappa \tag{2.4}$$

where

n - real part of the refractive index and is related to the phase velocity of electromagnetic waves in the material.

κ - imaginary part of the refractive index and is also known as the extinction coe□cient, which indicates the amount of attenuation (absorption) of the wave as it travels through the material.

2.1.2 Permittivity

Permittivity is defined as the amount of electric charge a material can hold. There exists a direct relation between complex permittivity and the refractive index of a material which is given by ($\varepsilon_r = n^2$). The equation for complex permittivity is similar to Eq. 2.4 but with a negative imaginary part. Here, ε and ε represent the real and imaginary parts of the complex permittivity [6].

$$\varepsilon = \varepsilon - j\varepsilon = \tilde{n}^2 \tag{2.5a}$$
$$\varepsilon = n^2 - \kappa^2 \tag{2.5b}$$
$$\varepsilon = 2n\kappa \tag{2.5c}$$

Real part of complex permittivity (ε): The real part of the complex permittivity quantifies the material's dielectric polarisation capacity which results from the displacement of charged particles within the material. A higher value of the real part implies that the material is a better insulator (or dielectric) because it can store more electric energy.

Imaginary part of complex permittivity (ε): The imaginary part of the complex permittivity, often termed the dielectric loss factor, reflects the material's capacity to dissipate energy, usually in the form of heat, when subjected to an electric field.

2.1.3 Loss tangent

Loss tangent ($\tan\delta$) is a dimensionless quantity which elaborates how much energy in a wave is lost to the medium through which it travels. It is mathematically expressed as [7],

$$\begin{aligned} \tan\delta &= \frac{\omega\varepsilon + \sigma}{\omega\varepsilon} \\ &\approx \frac{\varepsilon}{\varepsilon} \quad \text{when } \omega\varepsilon \quad \sigma \end{aligned} \tag{2.6}$$

where,

ω is the angular frequency

σ is the conductivity of the medium

The term $\omega\varepsilon + \sigma$ is considered as the total effective conductivity. For higher loss tangent, the material dissipates more energy when subjected to an electromagnetic field, which could be unfavourable in high-frequency applications due to increased heating and energy loss, and vice versa for material with low loss tangent.

The variations in permittivity and loss tangent among recycled plastics can be attributed to factors such as impurities, the molecular structure, and the processing methods employed during recycling. Understanding these parameters is pivotal for optimising the use of recycled plastics in various electromagnetic and electronic applications.

2.2 Measurement technique

Free-space transmission and reflection method is a widely used technique for measuring the dielectric properties of both homogeneous and heterogeneous samples. This method involves measuring the transmitted and reflected signals when the material is placed in the path of an electromagnetic (EM) wave. To calculate the permittivity, the transmitted and reflected signals are compared with the signals obtained when the wave propagates through free space. By analysing the phase and amplitude of these signals, the permittivity and loss tangent of the material can be determined. One of the key advantages of this method is its non-destructive nature, as it does not require physical contact with the material as in Fig. 2.1 [8]. Additionally, the free-space transmission and reflection method allows for measurements at various frequencies, providing a comprehensive characterisation of the material's electrical properties [8].

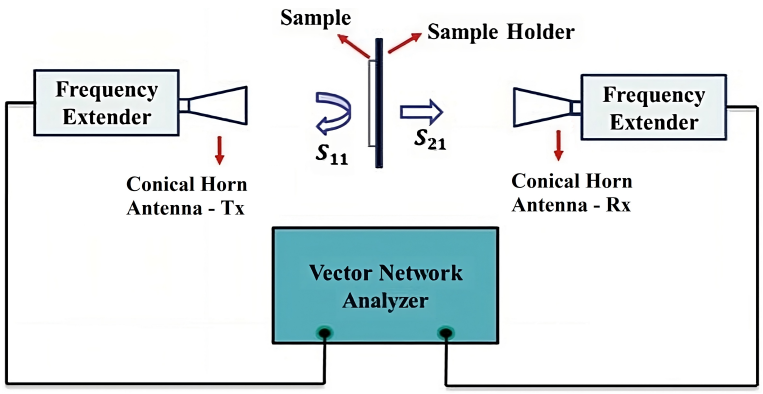

Figure 2.1: Free-space measurement method setup

The calibration method commonly used is the Short-Open-Load-Thru (SOLT) calibration [9]. SOLT calibration involves using known standards, such as short circuits, open circuits, and matched loads, to establish reference points for the measurement system. These standards are connected to the measurement setup, and their responses are measured and used to characterise the system's inherent errors and uncertainties [10]. The SOLT calibration method is widely recognised and used in

VNAs for accurate measurements of permittivity and loss tangent. It allows for the removal of systematic errors introduced by the measurement setup, ensuring reliable and precise characterisation of the material under test. Other calibration methods, such as Thru-Reflect-Line (TRL) and Thru-Reflect-Match (TRM), are also used in certain applications, but SOLT calibration is commonly employed due to its simplicity and e□ectiveness.

However, in the millimetre or sub-millimetre wavelengths, methods such as free-space measurement and transmission line techniques become lossy and impractical for many applications. To overcome this challenge, a combination of free-space measurement technique with optical principles, leading to the method called 'quasi-optical,' is utilised. This method involves using reflective mirrors or lenses to focus and manipulate millimetre or sub-millimetre waves in a manner analogous to optical systems.

By employing quasi-optical techniques, it becomes possible to achieve precise control and steering of electromagnetic waves at these short wavelengths. Reflective surfaces, such as mirrors or lenses, are strategically placed to guide and shape the propagation of the waves, enabling the creation of complex beam patterns and facilitating e□cient signal transmission or reception as shown in Fig. 2.2. Also the quasi-optical technique helps in characterising dielectric properties in a non-invasive and contact-less manner [11].

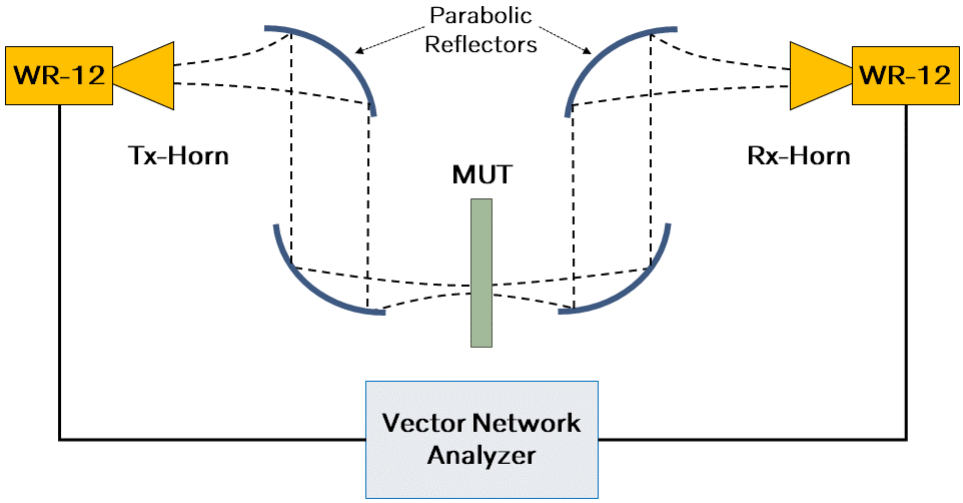

Figure 2.2: Quasi-optical measurement setup

In quasi-optical measurement technique, Transverse Electromagnetic (TEM) modes are used, preferably the TEM_{00} mode also known as the fundamental transverse mode which has a Gaussian beam profile with a single lobe and a constant phase across the mode. It is the lowest-order mode in a laser resonator and is commonly used in various applications, including dielectric measurements. The TEM_{00} mode is particularly useful because it provides a well-defined and easily characterised beam

profile, making it easier to extract accurate measurements of the dielectric properties of materials [12] [13].

The materials used for reflection, refraction, and other manipulations in the optical realm, such as glass and plastic, may not be as e□ective in the millimetre-wave or terahertz spectrum. One contributing factor is that materials like glass and plastic can exhibit high losses or sub-optimal transmission properties in the terahertz range. In contrast, metals demonstrate low losses in both the millimetre-wave and terahertz spectrum's, rendering them well-suited for manipulating electromagnetic waves within this frequency range. Their conductive characteristics make them suitable to use as lenses within quasi-optical systems operating in these frequency bands.

3

Method

This chapter briefly explains the ideology of analysing a test material of a certain thickness under a wide range of frequencies mostly between 65-90 GHz using the quasi-optical setup. The S-parameter data obtained from the VNA is verified against the analytical method of calculating the transmission S-parameter S_{21} through the transmission and reflection coe□cients. Through this comparison, the robustness of the calculation method for dielectric properties is verified and the calibration or calculation errors are rectified if found. The permittivity and loss tangent values obtained at 77 GHz is the only consideration for the finalisation of this research.

3.1 Principles of measurement

In electromagnetic theory, when a wave interacts with a material in its path of propagation, part of the wave is reflected back, and part of it is di□racted into the material. The reflection and transmission coe□cients are complex values that describe the amplitude and phase changes when passing along the MUT. This transmission and reflection of EM waves along their propagation path can be described using the Fresnel equations. The Fresnel reflection and transmission coe□cients for perpendicular (or normal) incidence are simpler in form compared to oblique incidence.

For a material with thickness, d, the interaction with the EM waves can be quite intricate. As a wave penetrates the material, it experiences multiple reflections within the layers, leading to a pattern of interference. In order to have the benefit of non-contact and non-destructive testing, the quasi-optical measuring technique is used to analyse the dielectric properties of the material at millimetre or sub-millimetre wavelengths. By measuring the amplitude and phase changes of both the reflected and transmitted EM waves, the complex refractive index of the material can be calculated using the Fresnel equations. The obtained complex refractive index value can be used to calculate the permittivity and loss tangent of the MUT.

3.2 Design of quasi-optical setup

The measurement setup in this thesis employs quasi-optical principles, specifically designed for Gaussian beam optics. Typically, to mitigate beam divergence between the antennas, metallic parabolic mirrors or dielectric lenses are employed [13]. In the quasi-optical configuration, the integration of metallic reflectors, often composed

of materials like aluminium or gold, plays a crucial role in shaping the parabolic or elliptical surfaces to achieve collimation of the Gaussian beam. These reflectors are carefully shaped into surfaces that possess the ability to reflect incident waves (gaussian, planar or circular) parallel to the optical axis, resulting in a collimated beam. Maintaining collimation is important in this setup, ensuring that the Gaussian beam retains its shape and traverses the material without significant distortion. Potential sources of distortion, such as beam divergence, di□raction, or scattering, can be mitigated by the use of metallic reflectors to collimate the beam. This approach minimises distortions, facilitating accurate analysis of the dielectric properties of the material.

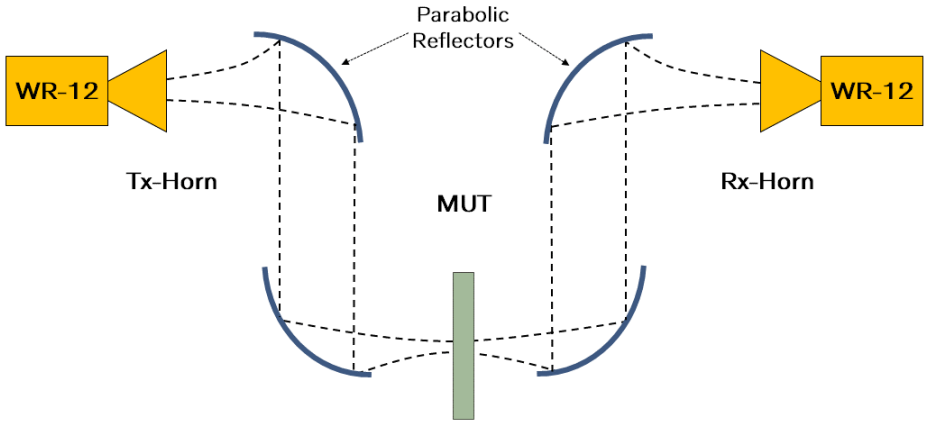

Figure 3.1: Schematics of the measurement setup

The aperture radius of the conical horn antennas is 19.9 mm and the beam waist radius (w_0) is 7.6 mm. The focal distance (76.2 mm) to mirror diameter (50.8 mm) ratio is 1.5. Using the parabolic reflective mirror, the beam from the Tx-horn antenna (or frequency extender) is collimated and made to interact with the MUT. The refracted beam through the MUT is made to focus on the Rx-horn antenna using the same type of reflectors in a mirrored manner as shown in Fig. 3.1.

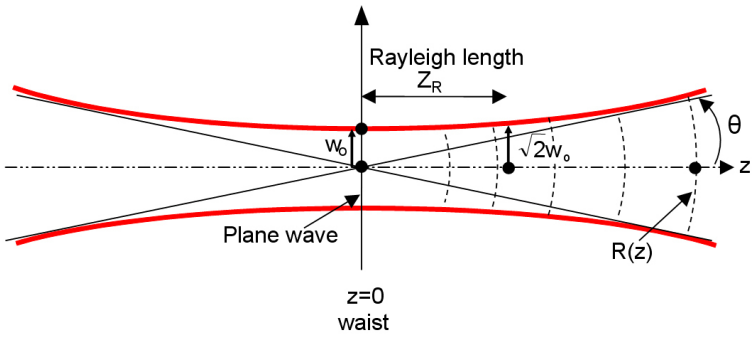

Figure 3.2: Properties of a Gaussian beam

The reason for using Gaussian beams, also known as TEM_{00} mode beams, is because of their unique intensity profile that follows a Gaussian distribution [14]. The gaus-

sian beam can be characterised by its beam waist (w_0) and divergence (θ), which are related to each other through the following equation,

$$\theta = \frac{\lambda}{(\pi w_0)} \tag{3.1}$$

where λ is the wavelength of the beam. As θ is represented under far-field conditions, its accuracy in representing the divergence of the beam improves as the distance from the beam waist increases [15]. But due to diffraction, the beam waist keeps varying along the direction of propagation. So the beam radius ($w(z)$) at position z (propagation distance) is expressed as,

$$w(z) = w_0\sqrt{1 + \left(\frac{z}{z_R}\right)^2} \tag{3.2}$$

where z_R is the Rayleigh range. The Rayleigh range is the distance z at which the cross-sectional area of the beam waist, the beam radius is increased by a factor of the square root of 2 as shown in Fig. 3.2 [16] [17]. For Gaussian beam it is given by

$$z_R = \frac{\pi w_0^2}{\lambda} \tag{3.3}$$

Fig. 3.3 shows how exactly the setup was designed to collimate the Gaussian wave propagation.

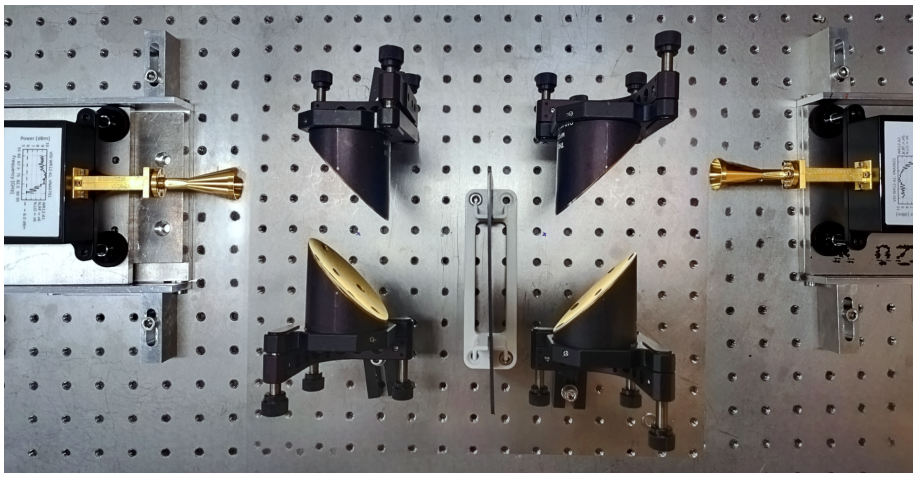

Figure 3.3: Quasi-optical measurement setup

When performing component characterisation tests, a network analyzer sends calibrated stimulus signals to the RF network and uses phase and amplitude information to measure the vector response over the chosen frequency. Signal sources and receivers are both included in network analyzers. Receivers detect changes in a device network's output signal and compare it to the source signal input into that device. The VNA examines both the amplitude and phase responses induced by the device to evaluate its effect on current and voltage. This helps in characterising the MUT

using the transmission and reflection measurements, impedance, and s-parameters that result. The VNA is calibrated by using the Short, Open, Load, Thru (SOLT) technique [9] [10] to get rid of the standing waves and mistakes brought on by multiple reflections when connecting the horn antenna to the frequency extenders. Removing this step might lead to a robust calibration, saving the temporal band-pass filter from having to be adjusted for each material.

Each frequency sweep took less than ten seconds. During the measurements, the temperature ranged between 22.6°C and 22.9°C. The specifications of the setup that were used in this thesis are tabulated below.

Instrument	Specification
Frequency Extender	Series: WR-12
	Frequency range: 60-90 GHz
Vector Network Analyzer	PNA - X
	Model: N5247B
	Output power: 6 dBm - 13 dBm
	Frequency range: 10 MHz - 67 GHz
	Port configuration: 2 and 4
	System dynamic range: 110 dB
	IF Bandwidth: 15 MHz
	Channels: 32
Off-axis parabolic mirrors	Series: MPD239-M01
	E□ective focal length: 15 mm (0.59") to 228.6 mm (9")
	Parent focal length: 38.1 mm
Sample Holder	Polypropylene
Antenna	Conical horn antenna
	Model - RCHO12R
	Aperture radius - 19.9 mm
	Beam waist radius - 7.6 mm
	Focal distance to mirror - 76.2 mm

Table 3.1: Specifications of apparatus used in the experimental setup

3.3 Signal flow analysis of setup

The signal flow analysis of the measurement system involves analysing how the VNA determines the transmission parameters. From Fig. 3.4, the incident waves of voltage are denoted by $\mathbf{a1}$ and $\mathbf{a2}$, while the reflected waves of voltage are denoted by $\mathbf{b1}$ and $\mathbf{b2}$. The matrices [A] and [B] represent the two-port network S-parameters of the optical path transition and the dielectric substrate slab, respectively, as shown

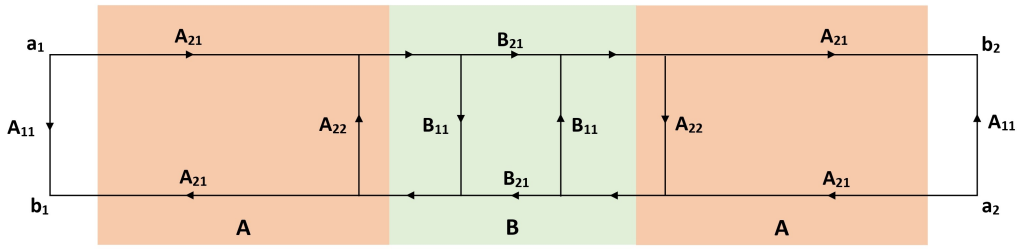

Figure 3.4: Signal flow graph of a two-port network

in Fig. 3.4. The setup in this experiment is based on a two-port network system. As the MUT is passive and symmetric, $B_{11} = B_{22}$. Then S_{21} is given by,

$$S_{21} = \left.\frac{b_2}{a_1}\right|_{a_2=0} = \frac{A_{21}^2 B_{21}(1 - A_{22}B_{11})}{(1 - A_{22}B_{11})^2 - A_{22}^2 B_{21}^2} \tag{3.4}$$

As there is no reflection on the free-space boundary, the reflection coe□cient (A_{22}) is normally equal to 0 [18]. Under such conditions, S_{21} simplifies to,

$$S_{21}|_{A_{22}=0} = A_{21}^2 B_{21} \tag{3.5}$$

Here B_{21} is the transmission S-parameter of the plane wave that passes through the dielectric substrate slab. The forward transmission parameter represented by S_{21} is split into two parts namely S_{21}^{air} and S_{21}^{MUT} which represent measurements performed without and with the MUT using the VNA [18]. The calculation of B_{21}^{MUT} is done by using Eq. 3.11.

$$B_{21}^{\text{air}} = \exp\left(\frac{-j2\pi f d}{c}\right) \tag{3.6a}$$

$$B_{21}^{\text{MUT}} = \left(\frac{S_{21}^{\text{MUT}}}{S_{21}^{\text{air}}}\right) \cdot B_{21}^{\text{air}} \tag{3.6b}$$

where,

c - speed of light

f - frequency used in measurement

d - thickness of the MUT

3.4 Analytical model

Theoretical calculations of dielectric properties are crucial for understanding the fundamental principles underlying electromagnetic propagation within the MUT. Such calculations verify the accuracy of physically measured dielectric properties, detect computational errors, and identify calibration or instrumentation losses, especially when computing permittivity and loss tangent. In the previous section, the complex

refractive index, permittivity, and loss tangent are calculated from the physically measured S-parameters. To validate the robustness of the extraction code, the parameters S_{21} and S_{11} are manually calculated and cross verified with the results of physical measurements.

Consider a MUT with thickness d surrounded by free space. The impedance of free space is Z_0 and the impedance of the material is denoted by Z. The relation between the impedance of free space and the material is given by $Z = \frac{Z_0}{\tilde{n}}$, where $\tilde{n}$ is the complex refractive index of the MUT [19].

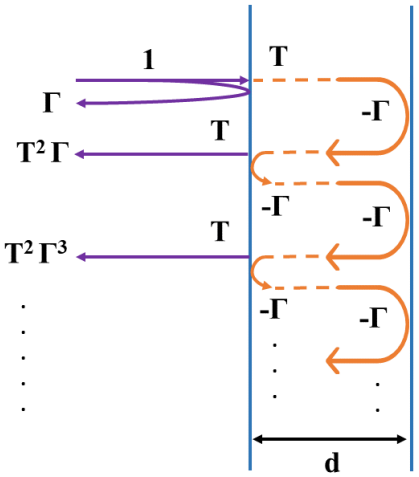

Figure 3.5: Transmission and Reflection coe□cient inside MUT

This relationship indicates the impact of a media with refractive index $\tilde{n}$ on its complex wave impedance, which in turn, a□ects the propagation of electromagnetic waves through the material. As an EM travels through an MUT, its amplitude and phase are altered due to its refractive index. This results in considering a reflection coe□cient (Γ) and a transmission coe□cient (T), at the interface between free-space and the MUT, as the wave exits the MUT back into free space as shown in Fig. 3.5. The reflection coe□cient Γ is a complex number that describes both the amplitude and phase change of the reflected wave and it is mathematically given by,

$$\Gamma = \frac{Z - Z_0}{Z + Z_0} \tag{3.7}$$

Substituting the relation of Z and Z_0 to Eq. 3.7

$$\Gamma = \frac{\frac{Z_0}{\tilde{n}} - Z_0}{\frac{Z_0}{\tilde{n}} + Z_0} = \frac{1 - \tilde{n}}{1 + \tilde{n}} \tag{3.8}$$

Now Eq. 3.8 is valid when the MUT is considered to have infinite thickness. But for a fixed thickness d, the transmission coe□cient (T) is given by [7],

$$T = 1 + \Gamma = \frac{2}{1 + \tilde{n}} \tag{3.9}$$

As explained above, when the EM waves follow multiple reflections inside the MUT having a thickness d, the transmission coe□cient T should include the propagation factor $e^{-j\beta d}$ as in [7]. But while considering complex refractive index of the MUT, it is changed to $e^{-jk_0\tilde{n}d}$. With this condition, the S_{21} from [20] is changed to,

$$S_{21} = \frac{(1 - \Gamma^2)e^{-jk_0\tilde{n}d}}{1 - \Gamma^2 \cdot e^{-2jk_0\tilde{n}d}} \tag{3.10}$$

where,

Γ is the reflection coe□cient given by Eq. 3.8

k_0 is the free-space wave number, given by $\omega\sqrt{\mu_0\varepsilon_0}$

d is the thickness of the MUT

3.5 Extraction of dielectric properties

When an MUT is influenced by EM waves, several factors must be considered to calculate its complex refractive index, including the e□ects of multiple reflections, phase changes, power loss due to reflections, and the magnitude and phase change of the reflected wave that passes through the MUT and returns to the transmitter. Normalising by the transmission through air accounts for the inherent transmission properties of the environment, thus isolating the e□ects of the MUT. This is mathematically expressed as,

$$\left(\frac{S_{21}^{\text{MUT}}}{S_{21}^{\text{air}}}\right)_m = \frac{(1 - \Gamma^2)}{1 - \Gamma^2 \cdot e^{(-2jk_0d\tilde{n})}} \cdot e^{-jk_0d(\tilde{n}-1)} \tag{3.11}$$

where $\tilde{n}$ is the complex refractive index.

In Eq. 3.11, the $(1 - \Gamma^2)$ term represents the power transmitted through the MUT, considering the power loss due to reflection (Γ). Since Γ is squared, it accounts for the power (intensity) reflection rather than just the amplitude. The exponential term $e^{-2jk_0d\tilde{n}}$ includes a complex exponent, which is indicative of the phase shift of the wave as it travels through the MUT twice (passing through and returning). Also the $e^{-jk_0d(\tilde{n}-1)}$ term accounts for the phase shift due to the di□erence in refractive index between the MUT and air (since air has a refractive index of approximately 1). It only considers the one-way trip through the material, not the return path.

To extract the complex permittivity and loss tangent value for each of the 10 materials, the following steps are done in order [21][18].

Step 1: Calculate B_{21}^{air} using Eq. 3.6a from the known parameters of the MUT.

Step 2: Use time-gating technique to selectively extract the transmitted signal through the MUT. The reason to do time-gating here is to separate the

reflected signal from the MUT, effectively isolating it from any subsequent reflections occurring between the horn antenna and the MUT.

Step 3: Using Eq. 3.6b, calculate B_{21}^{MUT} from the time-gated S_{21}^{MUT} and S_{21}^{air} from previous step.

Step 4: To get an initial guess of the refractive index, the phase (ϕ) and time delay (τ) of the transmission S-parameter is calculated from B_{21}^{MUT} across the entire frequency range through the equations given below.

$$\phi = \mathrm{Arg}(B_{21}^{\mathrm{MUT}}) \tag{3.12a}$$

$$\tau = -\frac{1}{2\pi} \cdot \frac{\Delta\phi}{\Delta f} \tag{3.12b}$$

$$n_i = \frac{\tau \cdot c}{d} \tag{3.12c}$$

Step 5: The physically measured and time-gated S_{21}^{MUT} and S_{21}^{air} is used to calculate $\left(\frac{S_{21}^{\mathrm{MUT}}}{S_{21}^{\mathrm{air}}}\right)_d$

Step 6: The value of complex refractive index is refined by the function

$$f(\tilde{n}) = \left(\frac{S_{21}^{\mathrm{MUT}}}{S_{21}^{\mathrm{air}}}\right)_m - \left(\frac{S_{21}^{\mathrm{MUT}}}{S_{21}^{\mathrm{air}}}\right)_d = 0 \tag{3.13}$$

Due to the periodic characteristics of the exponential components, Eq. 3.13 may yield several solutions. The initial estimate for the correct solution was based on the n_i value obtained in Step 4.

Step 7: Refine the estimate of the complex refractive index by minimising the error between the measured and a model-based calculation of the transmission coefficient for a range of possible refractive index values.

Step 8: Compute the real and imaginary parts of the permittivity from the refined refractive index estimates, subsequently determining the loss tangent from these values using Eq. 2.5b, Eq. 2.5c and Eq. 2.6

The application of time gating serves as a highly effective method for the isolation of the primary signal, effectively separating it from the undesirable influence of multiple reflections and interference. Each of the 9 samples was measured 5 times. The empty sample holder was measured before each sample measurement as a reference for relative measurements. Relative measurements reduced uncertainty caused by component misalignment, loss in the optical channel, and temperature and humidity variations.

4

Results

4.1 Materials used for analysis

The main purpose of this research is to measure the complex permittivity and loss tangent of recycled materials with different thicknesses in which a total of 10 materials (9 Recycled and 1 Non-recycled) are analysed. Most of the materials are composed of Polypropylene (PP), Polycarbonate / Acrolynitrile Butadiene Styrene (PC/ABS) and Polyphenylene Sulfide (PPS), they are tabulated below in Table.4.1

S.No	Name	Composition	Recycled
1	PP1	PP	Yes
2	PP2	PP	Yes
3	PP3	PP	Yes
4	PC1	PC/ABS	Yes
5	PC2	PC/ABS	Yes
6	PC3	PC/ABS	Yes
7	PC4	PC	Yes
8	PC5	PC	Yes
9	PC6	PC	Yes
10	PPS1	PPS	No

Table 4.1: Materials and their properties used in this research

4.2 Measurement results

In Microwave and Radio Frequency (RF) measurements, a common technique used particularly when characterising materials using S-parameters is dividing S_{21}^{MUT} by S_{21}^{air} during the initial raw data analysis. This is done to normalize the measurement, accounting for system characteristics like cable losses, connector losses, and other systematic errors. This process helps in isolating the effects occurring only due to the MUT, as the division effectively removes the system's baseline response. It also provides a relative measurement, comparing how the MUT alters the signal

in comparison to air. This comparison can be more insightful than absolute measurements, as it directly shows the impact of the material on the signal. By using air as a baseline, we can more accurately determine the material's impact on signal attenuation and phase shift. This is particularly useful in environments where absolute measurements might be difficult due to various uncertainties or instabilities in the setup.

4.2.1 Analysis of reference material PPS1

The reference material PPS1, derived from PPS (a high-performance thermoplastic renowned for its robustness, chemical resistance, and thermal stability), exhibits consistent properties representative of pure PPS due to its non-recycled nature. By using analytical methods to calculate the transmission coefficient (T) and reflection coefficient (Γ) of PPS1 within 65-90 GHz using Equations 3.8 and 3.9 and fixing its parameters like thickness d = 2.824 mm, permittivity ε = 3.17, and loss tangent $\tan\delta$ = 0.0134. The following plots explain their characteristics.

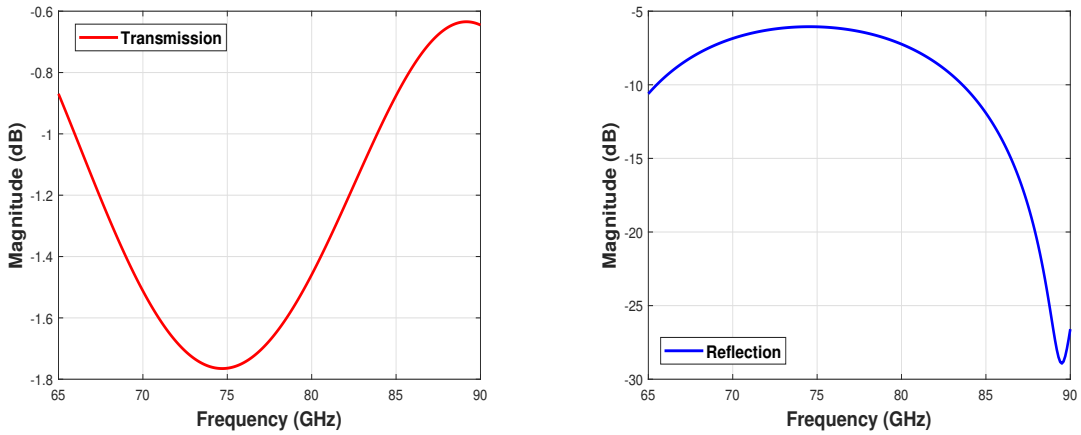

(a) Transmission coefficient using analytical model

(b) Reflection coefficient using analytical model

Figure 4.1: Transmission and reflection coefficients using the analytical model

In Fig. 4.1a, the transmission coefficient exhibits distinctive frequency-dependent attenuation in its entire propagation. Initially, it starts at -0.5 dB, dipping to -1.46 dB around 75 GHz, indicating increased absorption or reflection. Beyond this, it exponentially rises to 0.1 dB at 90 GHz, suggesting reduced attenuation at higher frequencies.

For the reflection coefficient as in Fig. 4.1b, that starts at -10 dB, peaks at -6 dB at 75 GHz, then exponentially decreases to -29 dB at 89.5 GHz, as the optical length of the slab is a multiple of the half of the the free space wavelength at 89.5 GHz. Now to extract the permittivity and loss tangent through the refractive index of the MUT, the raw data analysis is initially done and the magnitude and phase plots of the transmission parameter S_{21} is explained below.

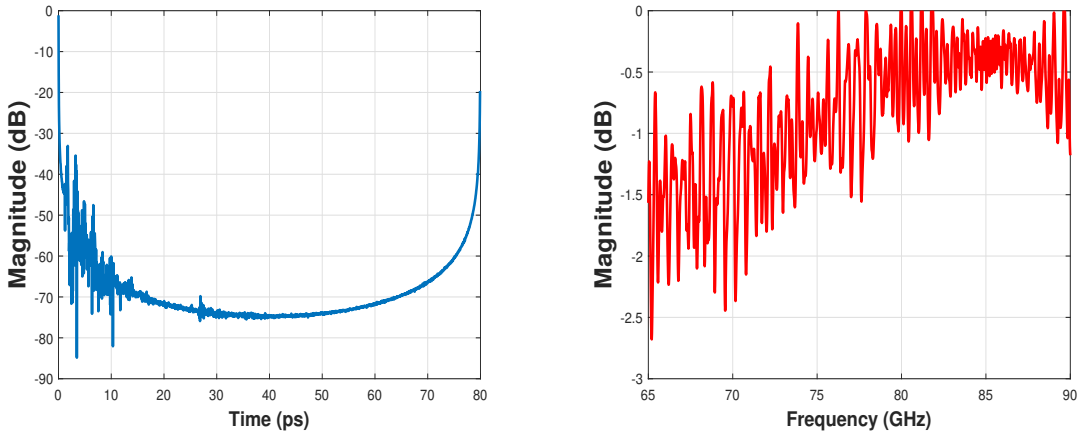

(a) Magnitude of normalised raw data in time domain

(b) Magnitude of normalised raw data in frequency domain

Figure 4.2: Normalised magnitude of PPS1: Time and Frequency domains

Fig. 4.2a and 4.2b show the magnitude responses of the normalised raw data in both time and frequency domain, here raw data refers to the normalised transmission coe□cient $\left(\frac{S_{21}^{MUT}}{S_{21}^{air}}\right)$. Multiple reflections on the MUT within the signal path are observed, as indicated by the presence of numerous peaks during propagation, which hinder the attainment of stable values. After applying time-gating to this normalised data to remove the reflections, the resulting magnitude and phase plots are plotted to illustrate their correspondence within the frequency domain.

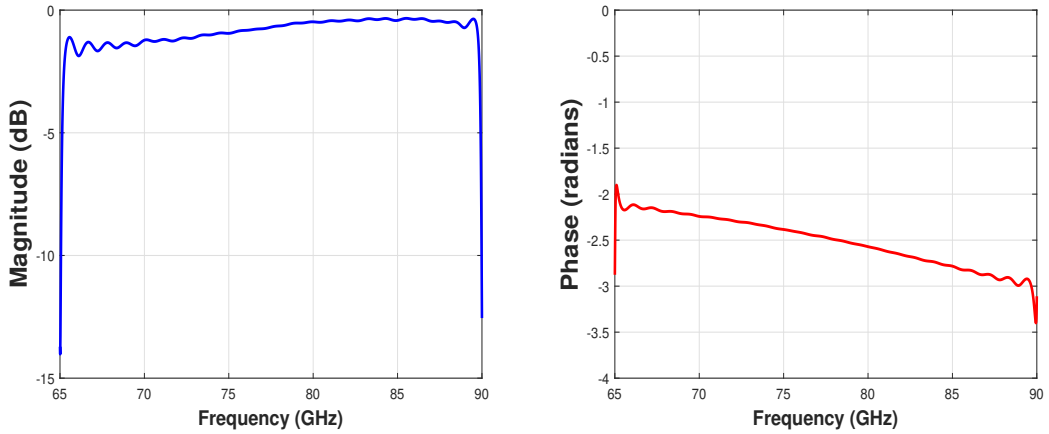

(a) Magnitude of time-gated normalised raw data

(b) Phase of time-gated normalised raw data

Figure 4.3: Time-gated normalised data for PPS1: Magnitude and Phase

From Fig. 4.3a, we observe that after applying time gating, the transmission coe□-cient is clearly visible across the entire frequency range of 68-88 GHz. Initially, it exhibits resonance, peaking early on, and then maintains full transmission up to 88

GHz. In Fig. 4.3b, initial phase shifts are evident, followed by a consistent phase delay persisting until 88 GHz. Subsequently, the refractive index of the MUT is calculated using the post-processed raw data.

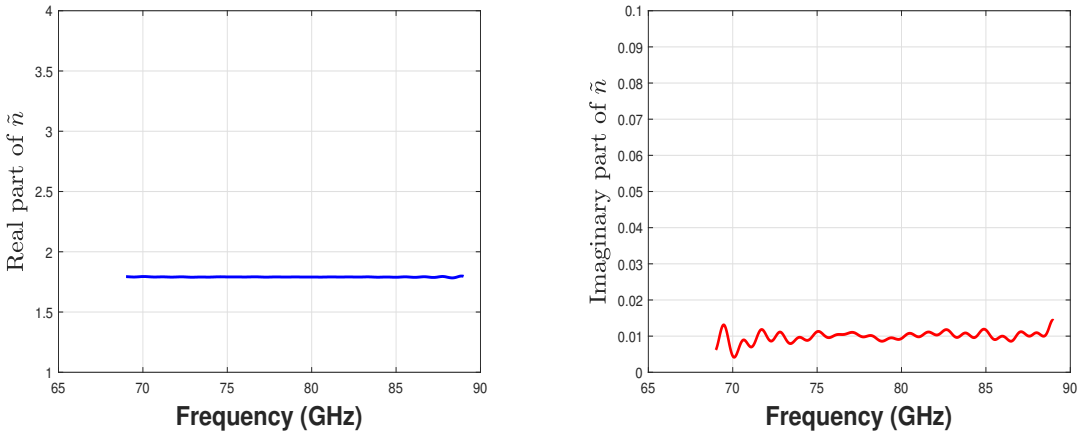

(a) Real part of complex refractive index

(b) Imaginary part of complex refractive index

Figure 4.4: Complex refractive part of PPS1: Real and Imaginary part

From the obtained refractive index values the complex permittivity is calculated through the equations 2.3, 2.5b and 2.5c. The plots are shown below.

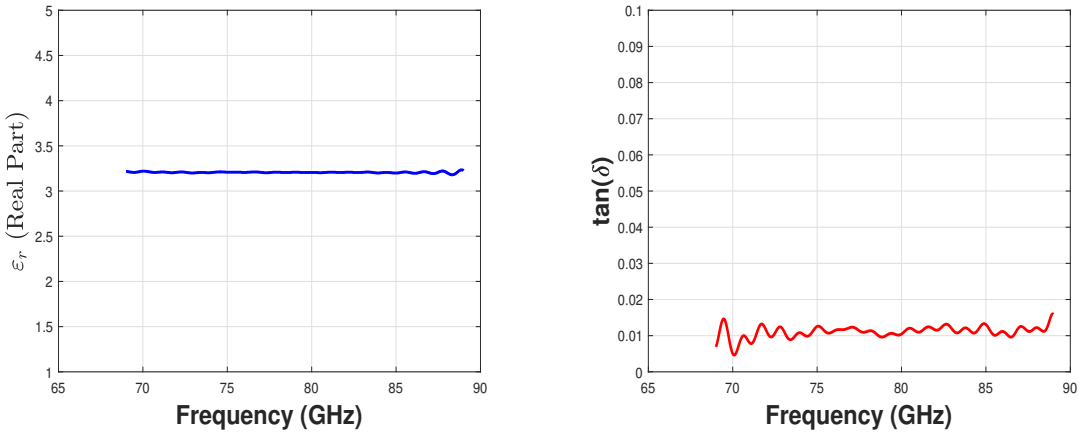

(a) Permittivity of PPS1

(b) Loss Tangent of PPS1

Figure 4.5: Permittivity and Loss Tangent of PPS1

It can be observed that the permittivity of PPS1 is approximately the square of the refractive index value obtained at 77 GHz. This finding clearly supports the fundamental relation between permittivity and refractive index as explained in Eq. 2.3. Furthermore, it indicates that the extraction method used for calculating the permittivity and loss tangent is robust.

4.2.2 Analysis of recycled sample PC6

This research primarily focuses on the dielectric properties of recycled materials that could be used in automobile parts. One such material is PC6, a Polycarbonate blend known for its usage in bumper manufacturing for its durability and impact resistance. Additionally, PC6 must be tested for its ability to allow radar signals to pass through and its impact on electromagnetic interference as they are essential factors for the e□ective operation of automotive radars.

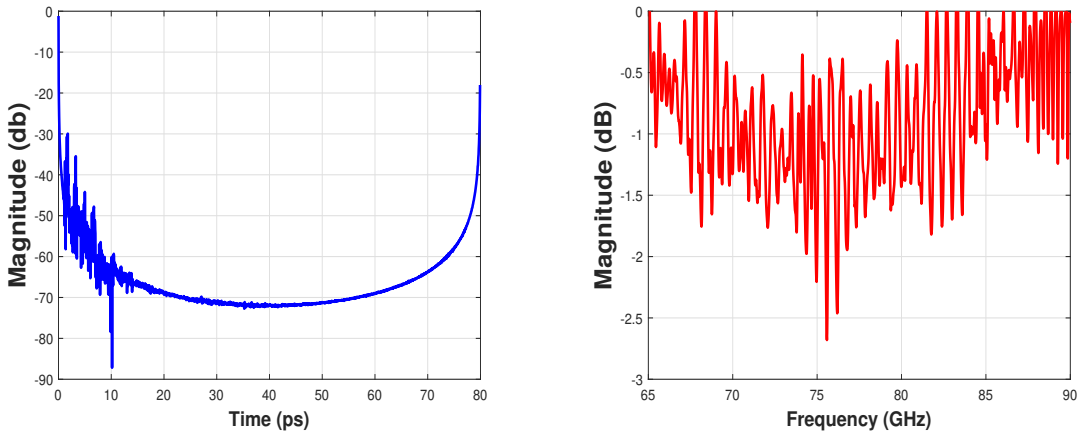

(a) Magnitude of normalised raw data in time domain

(b) Magnitude of normalised raw data in frequency domain

Figure 4.6: Normalised magnitude of PC6: Time and Frequency domains

In the analysis of PC6, multiple reflections are observed in the time domain as in Fig. 4.6a and in frequency domain as in Fig. 4.6b, which hinders the proper analysis of the material at such high frequencies. To eliminate these reflections, a 1.2 ns time gating window is applied across 69-88 GHz, aligning with the window size to minimise background e□ects as detailed in [22].

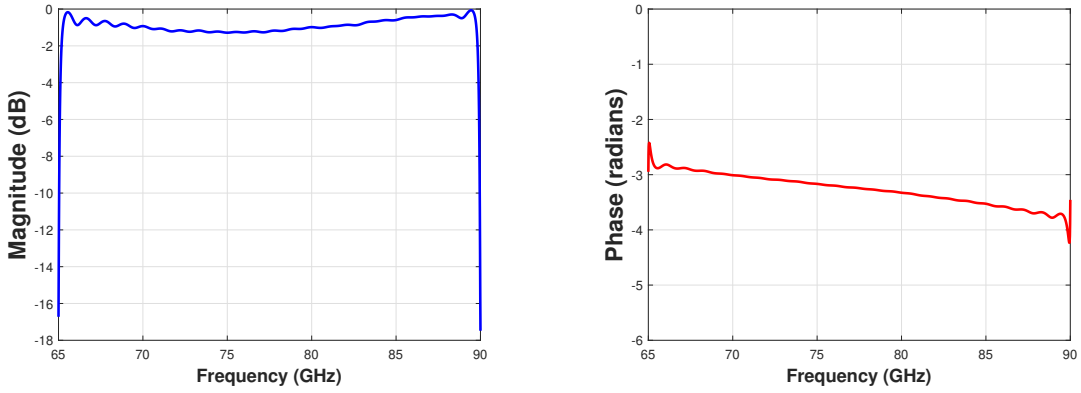

(a) Magnitude of time-gated normalised raw data

(b) Phase of time-gated normalised raw data

Figure 4.7: Time-gated normalised data for PC6: Magnitude and Phase

In Fig. 4.7a, after time gating, the transmission parameter quickly rises from -17 dB to 0 dB by 66 GHz, demonstrating minimal attenuation and e□ective signal transmission through most of the spectrum. The magnitude then declines to -1.8 dB at 75 GHz, possibly due to material properties or measurement errors, before sharply dropping back to -17 dB between 89 and 90 GHz, likely from material absorption or signal attenuation. In Fig. 4.7b, the phase begins at -2.95 radians at 65 GHz and slightly fluctuates, suggesting initial phase shifts. It declines steadily to -3.7 radians by 87 GHz, indicating consistent phase delay. Thereafter, it shows minor oscillations until 88 GHz, then quickly falls to -4.3 radians and peaks at -3.5 radians at 90 GHz, indicative of complex material behaviours or multi-path e□ects.

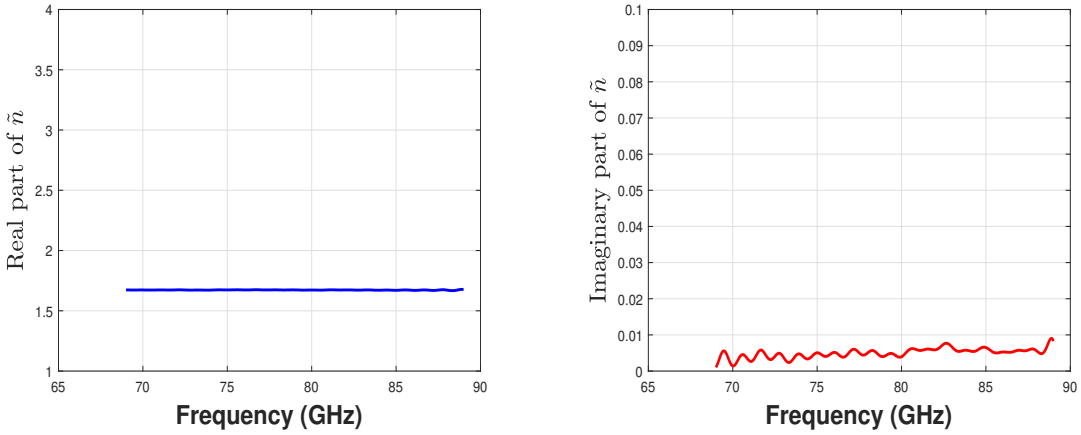

(a) Real part of $\tilde{n}$ for PC6 (b) Imaginary part of $\tilde{n}$ for PC6

Figure 4.8: Complex refractive index of PC6: Real and imaginary part

From Fig. 4.8a, it is observed that the real part of the complex refractive index (n), consistently measured as 1.65 across the entire frequency range, signifies that the test material possesses a stable and uniform optical density, irrespective of frequency variations.

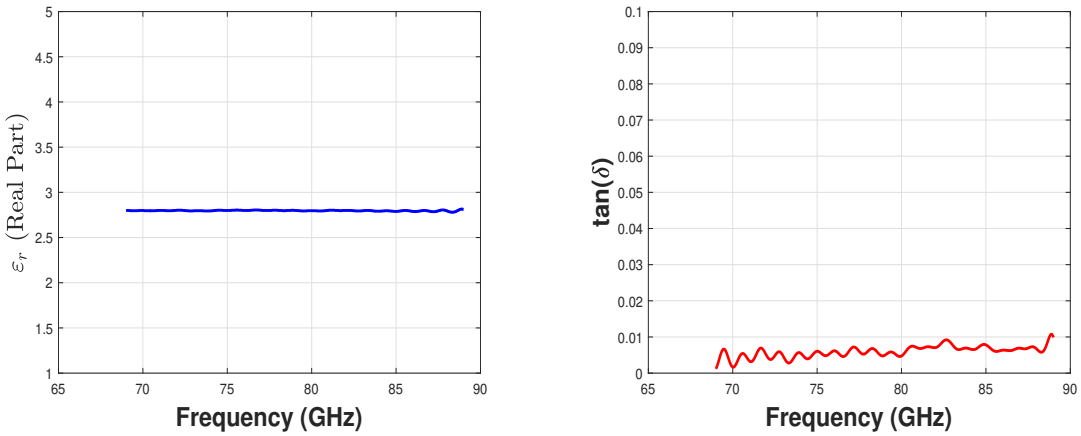

(a) Permittivity of PC6 (b) Loss tangent of PC6

Figure 4.9: Permittivity and loss tangent of PC6

The real part of the complex permittivity was found to be ≈ 2.817 as in Fig. 4.9a. When tanδ is low the energy loss due to dielectric heating is low. The loss tangent for PC6 was found to be 0.0146 at 77GHz as illustrated in Fig. 4.9b.

4.2.3 Multiple material analysis

In the final analysis of dielectric properties for the materials used in this research, S-parameters for each MUT were measured five times. The values for permittivity and loss tangent shown in Table.;4.2 for each material are the mean of these five readings. Averaging these measurements provides a more dependable result than a single reading, as it reduces the influence of any anomalies that might occur by chance.

The method of repeating measurements and averaging them is a standard practice in material testing to ensure accurate results. Even with careful control of experimental conditions, there can be small unavoidable variations. For instance, the positioning of the MUT could vary slightly with each measurement, or there might be undetectable di□erences in the material's consistency. Averaging helps to account for these minor inconsistencies, giving a more reliable indication of the materials' true properties and ensuring that the results are not skewed by any singular, unusual data point.

Material Name	Thickness (mm)	Permittivity	Loss Tangent
PP1	2.64	2.72	5e-3
PP2	2.63	2.74	8e-3
PP3	2.46	2.44	3e-4
PC1	3.18	2.80	6e-3
PC2	2.60	2.81	9e-3
PC3	2.20	2.73	8e-3
PC4	2.97	2.80	7e-3
PC5	2.97	2.82	5e-3
PC6	2.98	2.82	5e-3
PPS1	2.82	3.17	1e-2

Table 4.2: Permittivity and Loss tangent values measured at 77 GHz

While most materials shared a common real part, their loss tangents exhibited significant variation. This suggests that only a select few materials meet the design specifications suitable for use in bumper parts that shield automotive radar. Additionally, the analytical method employed in the analysis of these recycled plastics proves robust, consistently yielding the same supplier data after calculations for permittivity and loss tangent.

The figures depicted in Fig. 4.10 and Fig. 4.11 display the average of five-time measurements for both the real part and the tangential loss corresponding to each material.

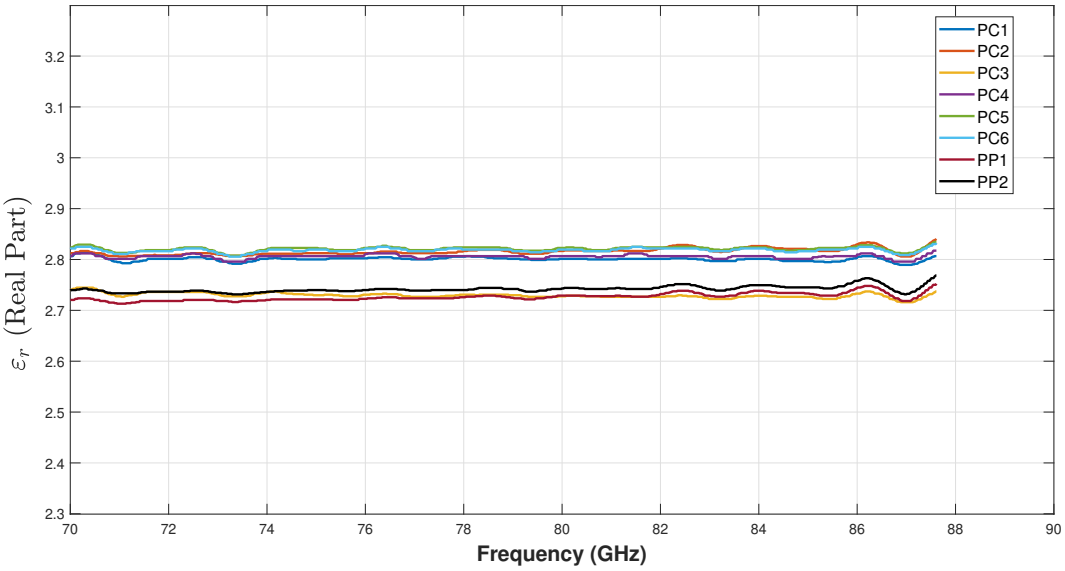

Figure 4.10: Permittivity of all test materials

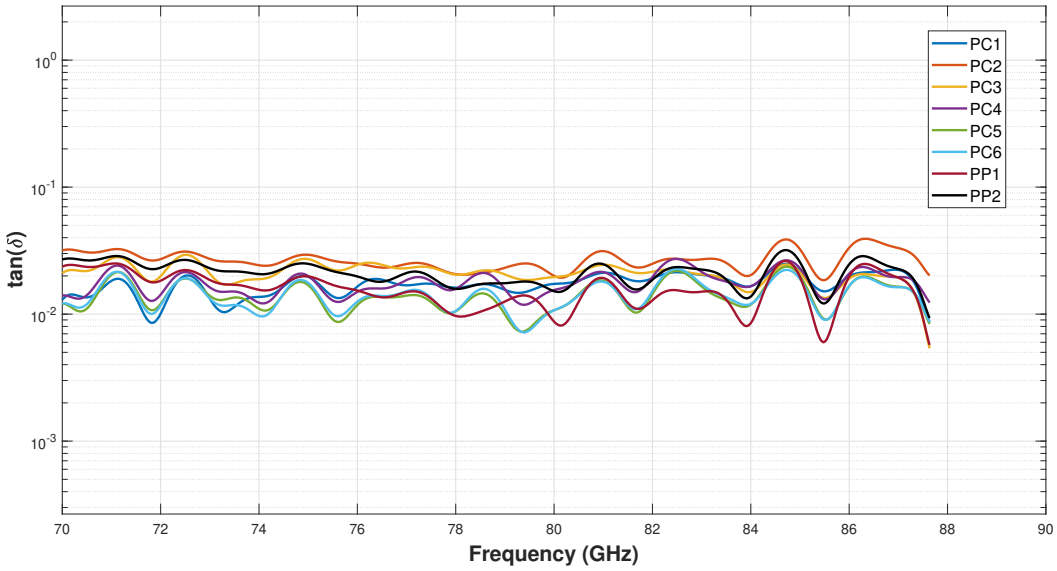

Figure 4.11: Loss tangent of all test materials

5

Conclusions

In the course of this thesis, a quasi-optical measurement technique combined with a vector network analyzer (VNA) was utilised to determine the electrical properties of recycled plastics accurately. The primary objective of this investigation is to gain insight into the real and imaginary components of the complex permittivity, as well as the loss tangent, by employing a robust design of experiment methodology. By meticulously gathering transmission data, it became feasible to accurately determine the permittivity values of recycled materials, thereby allowing for an in-depth evaluation of their dielectric attributes. Such a systematic approach is crucial for evaluating the electromagnetic behaviour of recycled plastics, making it possible to gauge their viability for diverse technological deployments.

The highlights of the quasi-optical measurement technique, with its swift and non-destructive nature, render it an exceptional tool for material characterisation. The structured methodology adopted can be delineated into the following phases:

- **Initial Measurements and Data Verification:** The research begins with preliminary measurements on reference material, the permittivity and loss tangent of which is already known. The derived permittivity and loss tangent values are then compared with the Original Equipment Manufacturer (OEM) specifications to confirm the integrity and accuracy of our extraction technique. This foundational step is paramount in ensuring that subsequent measurements are built upon verified data.
- **Extension to Various Materials:** Following the successful validation of our methodology, it is extended to encompass a wider range of test materials. This expansion enables precise measurements of both permittivity and loss tangent for di□erent substances, broadening the scope of applicability for the quasi-optical technique. The ability to characterise diverse materials is essential for comprehensive material analysis in various fields.
- **Theoretical calculation:** To further improve the robustness of our permittivity and loss tangent extraction process, we employ a comprehensive analytical approach. By using transmission, and reflection coe□cient equations while using two-port networks, we can theoretically calculate the permittivity and loss tangent values for the MUT.
- **Comparison of Analysis:** A comparison of physical and analytical computations is made with the empirical results derived from physical measurements. Discrepancies between the analytical calculations and physically mea-

sured data not only spotlight potential inaccuracies but also unveil any inherent biases or calibration challenges that might compromise result accuracy. An extensive alignment of analytical and empirical outcomes allows for an assertive validation of the precision and reliability of the computational tools used for determining permittivity and loss tangent.

Conclusively, the quasi-optical measurement technique, with its integrated approach that combines data validation, material extension, and comprehensive analysis, stands out as a potent tool for precise and dependable material characterisation. From the perspective of analysing the recycled plastic samples, materials with lower permittivity and loss tangent values are generally preferred for automotive radar applications at 77 GHz.

Among the tested materials, those with permittivity values closer to the reference material (PPS1) and lower loss tangent values exhibit better suitability for bumper manufacturing. Specifically, materials with permittivity values around 2.7 and lower loss tangent values, preferably below 8e-3, are considered more favourable. These characteristics contribute to minimal signal attenuation and interference, ensuring optimal radar performance in car bumpers.

The sustained and minimal variation in permittivity and loss tangent values observed across the recycled plastic samples emphasises their suitability for bumper production, a□rming their potential to contribute to the manufacturing of automotive radar-compatible bumpers with stable and reliable material characteristics.

6

Future work

6.1 Challenges and limitations

Recycled materials are often non-uniform, containing various components that make it hard to obtain a consistent sample for testing. These samples may have impurities a□ecting their dielectric properties, leading to inaccurate results if not considered. Preparing these materials for testing is critical but challenging due to their diverse nature, which can introduce errors if not done consistently. Moreover, recycled materials show frequency-dependent dielectric responses, necessitating measurements across a broad frequency range for accuracy.

The dielectric properties of materials like recycled plastics can change with temperature. Thus, keeping the temperature constant during tests is crucial for reliable results. Recycled materials can have high dielectric losses, particularly when they contain moisture or conductive elements, which can skew high-frequency measurements. Calibrating the equipment properly is essential, but finding suitable standards for recycled materials is di□cult due to their varied properties.

Interpreting data from these dielectric measurements is complex, especially for recycled composites with multiple phases. The lack of standardized methods for these materials makes it hard to compare results across di□erent studies. Moreover, advanced equipment required for some of these measurements, such as vector network analyzers, might be costly or unavailable in some research environments.

6.2 Characterisation and classification

When sorting and studying recycled plastics, it's important to look at both their physical and chemical characteristics to decide if they're right for certain products or market requirements. This includes checking how dense they are, how easily they melt and flow, how stable they are when heated, and whether they have any unwanted substances mixed in. These tests are crucial for figuring out if the recycled plastic is of good enough quality for its planned use. To understand how the material can be improved, it is required to look at how its physical and electrical properties, like its ability to store and lose electric charge, change over time. For instance, we can use modern scanning techniques that don't damage the plastic and can quickly give us a lot of information. By combining these methods with Machine Learning, we can get better at identifying and sorting di□erent types of recycled plastics, which can help make the whole recycling process more e□ective.

6.3 New measurement techniques

At present, the measurement of dielectric properties in recycled plastics often relies on outdated radar techniques that are not always precise and require a lot of data crunching. There's a shift towards using microwave imaging which promises to bring about a substantial improvement. This method provides real-time and more accurate measurements by using improved algorithms that can handle data swiftly. It's a straightforward approach that could significantly streamline the recycling process. By making the measurements more reliable, recycling becomes not only quicker but also more cost-e□ective. This is important for the environment, as better data leads to better recycling practices. Overall, the introduction of microwave imaging could be a game-changer in the way we recycle and reuse plastics.

6.4 Effects due to Plastic Processing

Plastic processing methods, such as extrusion and injection moulding, a□ect the material's physical and electrical characteristics. It's important to refine these methods to tailor the processing for specific applications. New techniques, including reactive extrusion and micro-injection moulding, allow for greater control over plastics' molecular structure and performance. These advances are particularly promising for sectors like electronics, automotive, and packaging. Continued research will enhance the sustainable use of plastics by deepening our understanding of the link between processing techniques and material properties.

Bibliography

[1] "Radio detection and ranging," *NATURE*, vol. 152, Oct. 1, 1943. DOI: 10.1038/152391b0. [Online]. Available: https://doi.org/10.1038/152391b0.

[2] A. Herrera. "Seven types of recyclable plastic: What is recyclable and non-recyclable." (Feb. 8, 2022), [Online]. Available: https://mikacycle.com/en/blogs/recyclable-and-non-recyclable.

[3] EuRIC - European Recycling Industries' Confederation, "Call for recycled content in plastics," 2023. [Online]. Available: https://euric-aisbl.eu/images/Position-papers/EuRIC-Call%5C%5Ffor%5C%5FRecycled%5C%5FContentPlastics.pdf.

[4] B. Max and W. Emil, *Principles of Photonics*. Cambridge University Press, 2019, ISBN: 9781139644181. [Online]. Available: https://doi.org/10.1017/CBO9781139644181.

[5] H. Gu, S. Zhu, B. Song, *et al.*, "An analytical method to determine the complex refractive index of an ultra-thin film by ellipsometry," *Applied Surface Science*, vol. 507, p. 145091, 2020, ISSN: 0169-4332. DOI: https://doi.org/10.1016/j.apsusc.2019.145091. [Online]. Available: https://www.sciencedirect.com/science/article/pii/S016943321933908X.

[6] M. Hallikainen, "Microwave dielectric properties of materials," in *Encyclopedia of Remote Sensing*, E. G. Njoku, Ed. New York, NY: Springer New York, 2014, pp. 364–374, ISBN: 978-0-387-36699-9. DOI: 10.1007/978-0-387-36699-9_100.

[7] D. M.Pozar, *Microwave Engineering 4th Edition*. 2011, p. 752, ISBN: 978-0-470-63155-3. [Online]. Available: http://alunoeletrica.eng.ufba.br/material/eletromagnetismoaplicado/livros/pozar.pdf.

[8] T. Ozturk and M. T. Güneşer, "Measurement methods and extraction techniques to obtain the dielectric properties of materials," in *Electrical and Electronic Properties of Materials*, M. K. Alam, Ed., Rijeka: IntechOpen, 2018, ch. 5. DOI: 10.5772/intechopen.80276.

[9] A. Kazemipour, J. Ho□mann, M. Wollensack, *et al.*, "Standard load method: A new calibration technique for material characterization at terahertz frequencies," *IEEE Transactions on Instrumentation and Measurement*, vol. 70, pp. 1–10, 2021. DOI: 10.1109/TIM.2021.3077660.

[10] K. Technologies, Aug. 22, 2023. [Online]. Available: https://rfmw.em.keysight.com/wireless/helpfiles/pxivna/S3_Cals/Select_Cal.htm.

[11] D. Bourreau, A. Peden, and S. Le Maguer, "A quasi-optical free-space measurement setup without time-domain gating for material characterization in the W-band," *IEEE Transactions on Instrumentation and Measurement*, vol. 55, no. 6, pp. 2022–2028, 2006. DOI: 10.1109/TIM.2006.884283.

[12] A. Kazemipour, S.-K. Yee, M. Hudlička, M. Salhi, T. Kleine-Ostmann, and T. Schrader, "Design and calibration of a compact quasi-optical system for material characterization in millimeter/sub-millimeter wave domain," in *29th Conference on Precision Electromagnetic Measurements (CPEM 2014)*, 2014, pp. 482–483. DOI: 10.1109/CPEM.2014.6898469.

[13] P. Goldsmith, "Quasi-optical techniques," *Proceedings of the IEEE*, vol. 80, no. 11, pp. 1729–1747, 1992. DOI: 10.1109/5.175252.

[14] R. Paschotta, *Gaussian beams*, RP Photonics Encyclopedia, Available online at https://www.rp-photonics.com/gaussian_beams.html, May 2005. DOI: 10.61835/mla. [Online]. Available: https://www.rp-photonics.com/gaussian_beams.html.

[15] E. Optics, *Gaussian beam propagation*. [Online]. Available: https://www.edmundoptics.com/knowledge-center/application-notes/lasers/gaussian-beam-propagation/.

[16] O. Ingenieur, *Physical properties of gaussian beams*. [Online]. Available: http://www.optique-ingenieur.org/en/courses/OPI_ang_M01_C03/co/Contenu_08.html.

[17] B. E. Saleh and M. C. Teich, *Fundamentals of Photonics*. John Wiley & Sons Inc, 2019. [Online]. Available: http://lib.ysu.am/disciplines_bk/1e50d8144d6e0c3ffea3ae655684c626.pdf.

[18] H.-T. Zhu and K. Wu, "Complex permittivity measurement of dielectric substrate in sub-thz range," *IEEE Transactions on Terahertz Science and Technology*, vol. 11, no. 1, pp. 2–15, 2021. DOI: 10.1109/TTHZ.2020.3036181.

[19] A. M. Nicolson and G. F. Ross, "Measurement of the intrinsic properties of materials by time-domain techniques," *IEEE Transactions on Instrumentation and Measurement*, vol. 19, no. 4, pp. 377–382, 1970. DOI: 10.1109/TIM.1970.4313932.

[20] S. Sahin, N. K. Nahar, and K. Sertel, "A simplified nicolson–ross–weir method for material characterization using single-port measurements," *IEEE Transactions on Terahertz Science and Technology*, vol. 10, no. 4, pp. 404–410, 2020. DOI: 10.1109/TTHZ.2020.2980442.

[21] A. Moradikouchi, A. Sparén, S. Folestad, J. Stake, and H. Rodilla, "Terahertz frequency domain sensing for fast porosity measurement of pharmaceutical tablets," *International Journal of Pharmaceutics*, vol. 618, p. 121579, 2022, ISSN: 0378-5173. DOI: 10.1016/j.ijpharm.2022.121579.

[22] I. Vakili, L. Ohlsson, L.-E. Wernersson, and M. Gustafsson, "Time-domain system for millimeter-wave material characterization," *IEEE Transactions on Microwave Theory and Techniques*, vol. 63, no. 9, pp. 2915–2922, 2015. DOI: 10.1109/TMTT.2015.2449833.

DEPARTMENT OF ELECTRICAL ENGINEERING
CHALMERS UNIVERSITY OF TECHNOLOGY
Gothenburg, Sweden
www.chalmers.se

CHALMERS
UNIVERSITY OF TECHNOLOGY